Optimization of Skyrmionic Magnetic Tunnel Junctions

Mengqi Zhao[1,2†], Aitian Chen[3,4†], Enlong Liu[5], Le Zhao[1,2] , Shasha Wang[5], Shikun He[5], Xixiang Zhang[3*], and Wanjun Jiang[1,2,6*]

[1]*State Key Laboratory of Low-Dimensional Quantum Physics and Department of Physics, Tsinghua University, Beijing 100084, China*
[2]*Frontier Science Center for Quantum Information, Tsinghua University, Beijing 100084, China*
[3]*Physical Science and Engineering Division, King Abdullah University of Science and Technology, Thuwal 23955–6900, Saudi Arabia*
[4]*State Key Laboratory of Electronic Thin Film and Integrated Devices, School of Physics, University of Electronic Science and Technology of China, Chengdu 611731, China*
[5]*Zhejiang Hikstor Technology Co. LTD., Hangzhou 311305, China*
[6]*Collaborative Innovation Center of Quantum Matter, Beijing 100084, China*

(Received 5 February 2025; accepted manuscript online 5 March 2025)

Magnetic skyrmions are recognized as potential information carriers for building the next-generation spintronic memory and logic devices. Towards functional device applications, efficient electrical detection of skyrmions at room temperature is one of the most important prerequisites. Magnetic tunnel junctions (MTJs) offer a technologically feasible solution by using spin-dependent tunneling of electrons, which can output the presence and absence of skyrmion as the pronounced tunneling magnetoresistance (TMR). However, a successful integration of skyrmionic films with MTJ stacks, together with the subsequent electrical detection of mobile skyrmions, is limited by several important factors, which will be systematically addressed in this study. In particular, we will show our optimization strategy of integrating the multilayer $[Pt/Co/Ta]_{10}$ that hosts room temperature skyrmions, with the Ta(spacer)/$CoFeB_1$/MgO/$CoFeB_2$ MTJ stack that exhibits a perpendicular magnetic anisotropy (PMA). By changing the thickness of the Ta spacer, we establish a ferromagnetic coupling between the $[Pt/Co/Ta]_{10}$ multilayer and the bottom $CoFeB_1$ free layer, which is critical for imprinting room-temperature skyrmions from the $[Pt/Co/Ta]_{10}$ multilayer into the free layer of the MTJ stack. The skyrmionic MTJ stack is further optimized by changing both the thickness of the bottom $CoFeB_1$ layer and the annealing temperature. As a result, a TMR ratio of 100% and the electrical signature of the skyrmion phase are successfully obtained at room temperature. Our optimization strategy of the skyrmionic MTJ stack and enhanced performance of skyrmionic MTJ devices could accelerate the exploration of skyrmionic memory and logic devices.

DOI: 10.1088/0256-307X/42/4/047502 CSTR: 32039.14.0256-307X.42.4.047502

Introduction. Magnetic skyrmions are topological quasiparticles, which feature intriguing physics and exhibit potential for the next-generation spintronic memory and computing devices.[1–13] In particular, Néel-type skyrmions in asymmetric magnetic multilayers can be stabilized at room temperature and manipulated by the current-induced spin-orbit torques (SOTs), which are envisioned to be advantageous for technological applications.[14–17] In addition to the deterministic generation and manipulation of skyrmions, an efficient electrical detection of skyrmions is equally important.[7,9,10,18–21] Recent efforts have been made in this latter direction, including the electrical detection of skyrmions by the Hall and Nernst effects,[18,22–25] along with many different approaches.[26–29] However, the detection of the presence and absence of skyrmions with the pronounced resistance differences remains challenging, thereby impeding the implementation of skyrmions in relevant applications.

Magnetic tunnel junctions (MTJs) consist of two magnetic layers that are separated by an insulating tunneling barrier.[30–34] The spin-dependent quantum tunneling of electrons between the parallel and antiparallel magnetization configurations gives rise to drastically different low and high tunneling magnetoresistance (TMR) states. Numerous early studies have identified the $CoFeB_1/MgO/CoFeB_2$ trilayer as one of the pivotal candidates for hosting large TMR ratios,[31,35,36] as well as for enabling nanoscale MTJ devices with perpendicular magnetic anisotropy (PMA).[33,37,38] Based on these important developments, MTJs have been incorporated as a building block of the magnetic random access memory (MRAM) technology.[39] Given that the TMR effect can convert the parallel and antiparallel magnetization configurations into significant resistance differences, it has naturally been considered advantageous for the efficient electrical detection of skyrmions.[9,40–52] This topic is of active

†These authors contributed equally to this work.
*Corresponding author. Email: xixiang.zhang@kaust.edu.sa; jiang_lab@tsinghua.edu.cn
© 2025 Chinese Physical Society and IOP Publishing Ltd. All rights, including for text and data mining, AI training, and similar technologies, are reserved.

research, on which several important results have been recently reported.[47–53] However, a systematic study of how nanoscale skyrmions in multilayers can be integrated with the MTJ stack, and how to increase the accompanied TMR ratio, remain to be thoroughly explored.

In this work, we optimize skyrmionic MTJ multilayers by integrating the skyrmion-hosting multilayer $[Pt/Co/Ta]_{10}$ with the perpendicularly magnetized MTJ of stacking order Ta(spacer)/$CoFeB_1$/MgO/$CoFeB_2$, and a synthetic antiferromagnet (SAF) of stacking order $[Pt/Co]_2$/Ru/$[Co/Pt]_3$. By changing the thickness of the Ta spacer (that is inserted between the $[Pt/Co/Ta]_{10}$ multilayer and the bottom $CoFeB_1$ free layer), as well as the thickness of the bottom $CoFeB_1$ free layer, we achieve a ferromagnetic coupling between them. This is crucial for enabling an imprinting of Néel skyrmions into the bottom $CoFeB_1$ free layer of the top-pinned MTJ stack.[54–56] Through performing minor loop measurements, we show that these skyrmionic MTJ devices are capable of detecting skyrmions at room temperature. We further study the TMR ratio as a function of annealing temperature, which reaches a maximum of 112.3% at 300 ℃. Compared with the bottom-pinned MTJs used in spin transfer torque (STT) devices,[33,42,49,57] these top-pinned MTJ structures are compatible with TMR readout of mobile skyrmions driven by SOTs.[45,46,51,53,56] Our optimization strategy of the top-pinned skyrmionic MTJs could be important for implementing efficient skyrmion-based devices.

Design of the Skyrmionic MTJ Stacks. The skyrmionic MTJ stack structure is illustrated in Fig. 1(a). The stacks (from bottom to the top) are in the order of Ta(5)/$[Pt(2.5)/Co(1)/Ta(0.5)]_9$/Pt(2.5)/Co(1)/Ta($t_{Ta}$, spacer)/$CoFeB_1$($t_{CoFeB_1}$)/MgO(1.7)/$CoFeB_2$(1.1)/Ta(0.5)/Co(0.3)/$[Pt(1.5)/Co(0.4)]_2$/Ru(0.85)/$[Co(0.5)/Pt(1.5)]_3$/Ru(5) (thickness in nm). These MTJ stacks are deposited on thermally oxidized Si substrate using an ultrahigh vacuum magnetron sputtering system at room temperature (Singulus ROTARIS). Due to the broken interfacial inversion symmetry and the strong spin-orbit coupling of the involved heavy metal elements, the bottom $[Pt/Co/Ta]_{10}$ multilayers could host nanoscale Néel-type skyrmions at room temperature via the interfacial Dyzaloshinskii-Moriya interaction, together with the potential for the electrical manipulation of skyrmions through the current-induced SOTs.[15,58,59] MTJ multilayer of stacking order and composition Ta(t_{Ta}, spacer)/$CoFeB_1$(t_{CoFeB_1})/MgO(1.7)/$CoFeB_2$(1.1) is selected to ensure both the presence of PMA and the large TMR ratio. Through adjusting the thickness of the Ta spacer (t_{Ta}), the $[Pt/Co/Ta]_{10}$ multilayers and the bottom $CoFeB_1$ layer could form a hybrid free layer via interlayer coupling.[60,61] Note that the thickness of the MgO tunneling barrier is fixed at 1.7 nm in this work, which ensures a high-quality crystallization of the MgO layer and a well-defined interface between the CoFeB layers and the MgO layer.[31,33,35–37,62] The top Co(0.3)/$[Pt(1.5)/Co(0.4)]_2$/Ru(0.85)/$[Co(0.5)/Pt(1.5)]_3$ multilayer is a SAF with an exchange coupling field at

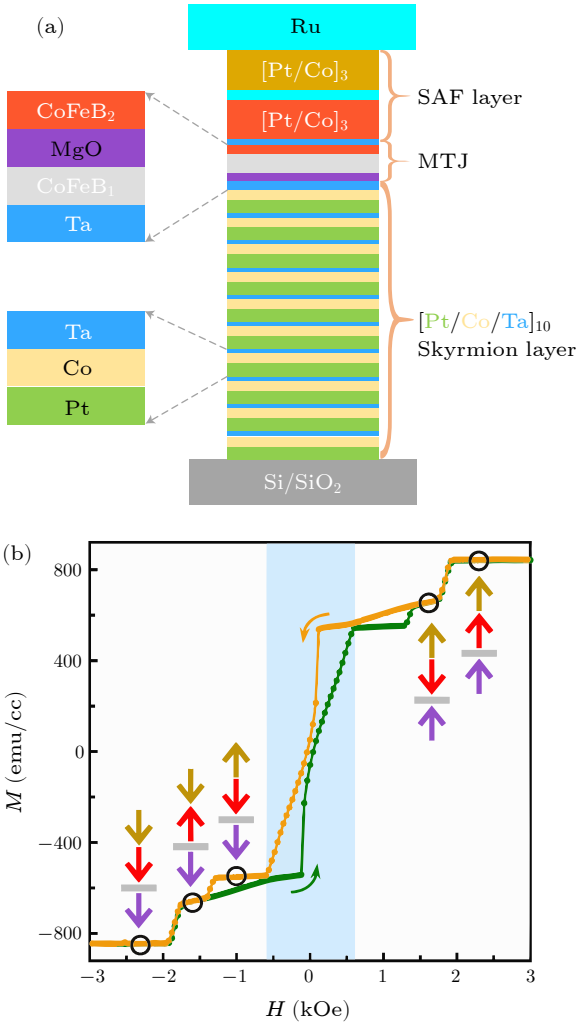

Fig. 1. (a) Schematic illustration of the skyrmionic MTJ stack. The skyrmion-hosting multilayer is $[Pt(2.5)/Co(1)/Ta(0.5)]_{10}$ (thickness in nm). The free layer of the MTJ, represented by the bottom $CoFeB_1$ layer (purple), is ferromagnetically coupled with the $[Pt(2.5)/Co(1)/Ta(0.5)]_{10}$ multilayer, forming a single hybrid free layer of the skyrmionic MTJ. The reference layer of the MTJ, represented by the red $CoFeB_2$ layer, is pinned by the top SAF layer. (b) Out-of-plane magnetic hysteresis loop of the skyrmionic MTJ stack. The arrows indicate the magnetization orientations of different layers, following the sweeping of magnetic fields from the positive to the negtive direction. The purple, red, and brown arrows represent the $CoFeB_1$ free layer, the $CoFeB_2$ reference layer, and the upper $[Co/Pt]_3$ layers of the SAF, respectively. The shaded region corresponds to the magnetic signal of the $[Pt/Co/Ta]_{10}$ multilayers.

1.8 kOe, which pins the top $CoFeB_2$ (t_{CoFeB_2}) layer. The 5-nm thick Ru serves as a top electrode and capping layer. The optimization strategy is as follows:

(1) We will first show how the thickness of the inserted Ta spacer (t_{Ta}) influences the interlayer ferromagnetic coupling between the $[Pt(2.5)/Co(1)/Ta(0.5)]_{10}$ multilayers and the bottom $CoFeB_1$ layer.

(2) Secondly, the influence of the varied thicknesses of the bottom $CoFeB_1$ free layer (t_{CoFeB_1}) on both the strength of PMA and TMR ratio will be studied.

(3) Thirdly, the effect of the annealing temperature of MTJ

devices on the TMR ratio will be investigated.

The first step enables a ferromagnetic interlayer coupling between the skyrmion multilayer and the bottom free layer of the MTJ stack and ensure the crystalization of MgO tunneling barrier. The second step introduces the PMA of the $CoFeB_1$ free layer and facilitates an efficient conversion of skyrmion spin textures into the sizable TMR. The third step is required to maximize the TMR ratio, which is useful for electrical readout of the presence and absence of skyrmions.

Figure 1(b) shows the out-of-plane magnetic hysteresis loop ($M - H_z$) of a selected skyrmionic MTJ stack of the following order: Ta(5)/[Pt(2.5)/Co(1)/Ta(0.5)]$_9$/Pt(2.5) / Co(1) / Ta(1, spacer) / $CoFeB_1$(0.9) / MgO(1.7) / $CoFeB_2$(1.1)/Ta(0.5)/SAF (thickness in nm). This measurement is performed by using a superconducting quantum interference device (SQUID) magnetometer. The magnetization orientations of the bottom $CoFeB_1$ free layer, the top $CoFeB_2$ reference layer, and the upper $[Co/Pt]_3$ of the SAF (Co(0.3)/[Pt(1.5)/Co(0.4)]$_2$/Ru(0.85)/[Co(0.5)/Pt(1.5)]$_3$) are indicated by the purple, red, and brown inset arrows, respectively. When scanning the magnetic field from positive to negative (dark yellow curve), the magnetizations of the SAF layers first switch from being parallel to antiparallel at 1.8 kOe. As the magnetic field decreases further, the hybrid free layer undergoes a gradual switching. The shaded region represents the magnetic signal of the $[Pt/Co/Ta]_{10}$ multilayers, the shape of which is consistent with those typical multilayers that host Néel-type skyrmions.[15,17,59,63–65] At −1.3 kOe, the residual magnetic moment of the uncompensated SAF layers flips. Below −1.8 kOe, the magnetization of the SAF layers are aligned parallel with the field.

For TMR measurements, all multilayers are patterned into four-terminal devices with a pillar size of 3 µm in diameter, which are done by standard lithography.[66] The measurements are subsequently conducted using the four-terminal method and the standard lock-in technique, as shown in Fig. 2(a). Figure 2(b) illustrates the out-of-plane TMR loops for three selected MTJ stacks with varied thicknesses of the Ta spacer as follows: Ta(5)/[Pt(2.5)/Co(1)/Ta(0.5)]$_9$/Pt(2.5)/Co(1)/Ta(t_{Ta} = 0.8, 1.0, 1.4)/$CoFeB_1$(0.9)/MgO(1.7)/$CoFeB_2$(1.1)/Ta(0.5) /SAF (thickness in nm), as labeled in the inset. A precisely controlled thickness of the Ta spacer (t_{Ta}) is crucial for two key functions: (a) enabling a ferromagnetic coupling between the skyrmion multilayer and the bottom free layer of the MTJ stack, such that they behave as a single hybrid free layer, (b) ensuring the formation of high-quality MgO tunneling barrier to achieve a high TMR ratio.[60,61,67] After annealing at 250 ℃ for one hour, all three samples in Fig. 2(b) show PMA and sizable TMR ratios. In addition, a coherent switching is observed in the minor loops, which indicates that a hybrid free layer is established. Thus, a fixed thickness of t_{Ta} = 1 nm of the Ta spacer is selected for the subsequent optimization.

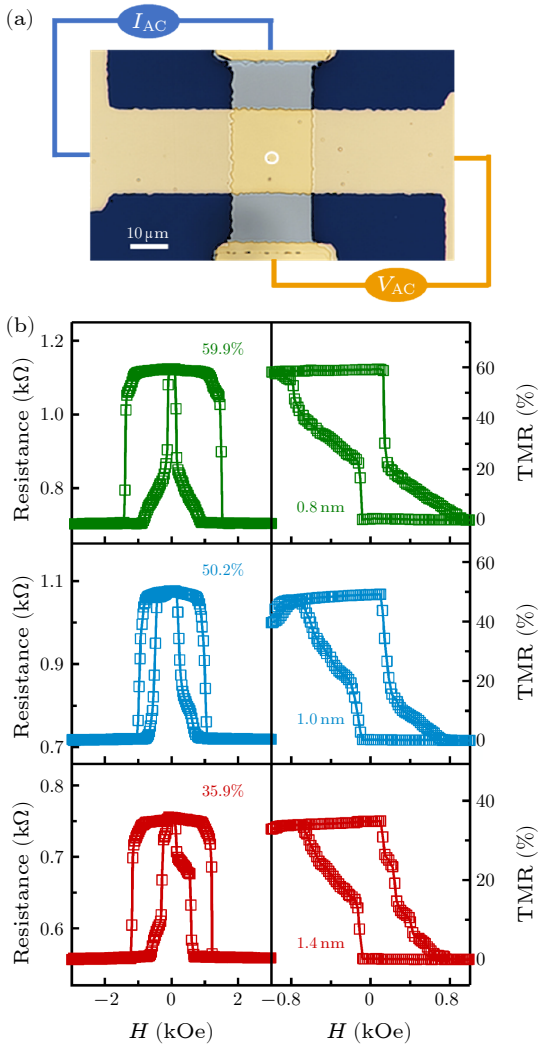

Fig. 2. (a) Optical microscopy image of an MTJ device and a schematic illustration of the four-terminal electrical measurement setup. The diameter of the MTJ pillar is 3 µm as indicated by the white circle. (b) Out-of-plane major (left) and minor (right) TMR hysteresis loops for three MTJ stack structures with varied thicknesses of the Ta spacer: Ta(5)/[Pt(2.5)/Co(1)/Ta(0.5)]$_9$/Pt(2.5)/Co(1)/Ta(t_{Ta} = 0.8, 1.0, 1.4)/$CoFeB_1$(0.9)/MgO(1.7)/$CoFeB_2$(1.1)/Ta(0.5)/SAF (thickness in nm).

Variation of TMR with the Thickness of the Bottom $CoFeB_1$ Layer. We proceed to optimize the skyrmionic MTJ stack by changing the thickness of the bottom $CoFeB_1$ free layer, for which influences both the strength of PMA and the ratio of TMR. In particular, the strength of PMA is strongly correlated with the thickness of the $CoFeB_1$ free layer, which subsequently modulates the strength of interlayer ferromagnetic coupling with the $[Pt/Co/Ta]_{10}$ multilayer.[54,68] This can be found from the shape of the minor loops. Various skyrmionic MTJ stacks are deposited with different thicknesses of the bottom $CoFeB_1$ free layer varying from 0.9, 1.05, 1.1, to 1.15 nm. These multilayers are thereafter fabricated into microscale MTJ devices of 3 µm-diameter pillars and annealed at 300 ℃ for one hour.

Figure 3(a)–3(d) show the corresponding major and minor TMR hysteresis loops. Here, the TMR ratio is

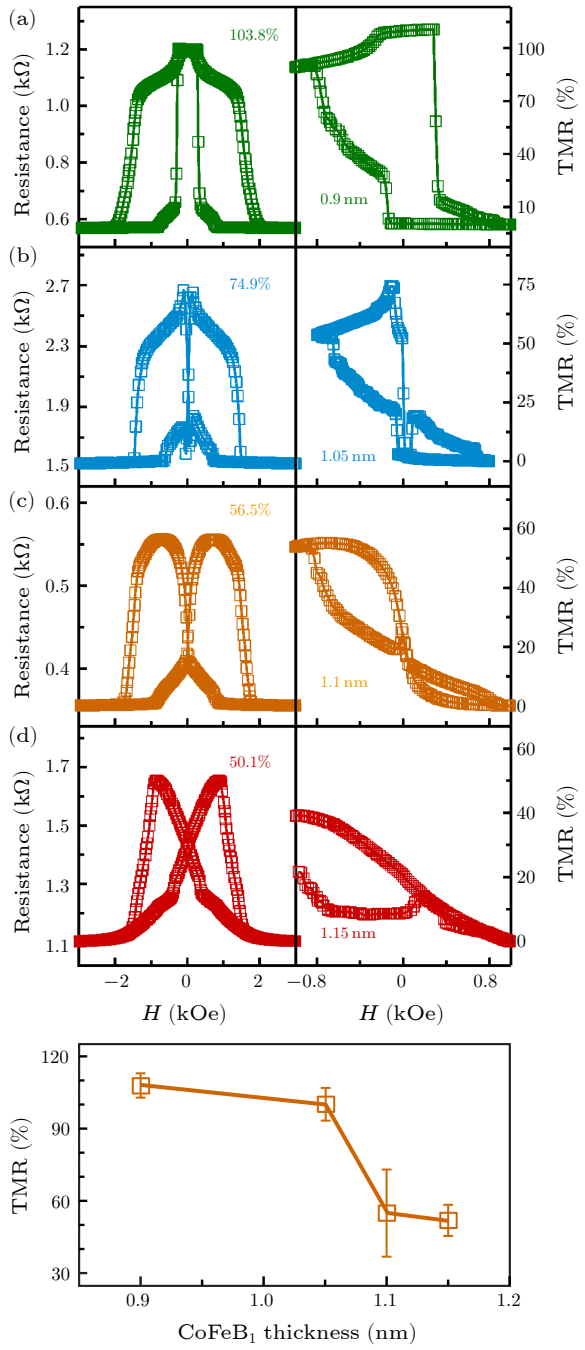

Fig. 3. (a)–(d) Out-of-plane major (left) and minor (right) TMR loops for MTJ devices with different thicknesses of the bottom $CoFeB_1$ free layer. Ta(5)/[Pt(2.5)/Co(1)/Ta(0.5)]$_9$/Pt(2.5)/Co(1)/Ta(1, spacer) /$CoFeB_1$(t_{CoFeB_1} = 0.9, 1.05, 1.1, 1.15)/MgO(1.7)/ $CoFeB_2$(1.1)/Ta(0.5)/SAF (thickness in nm). The thickness of the bottom $CoFeB_1$ free layer and the corresponding TMR ratio are labeled in the figure. (e) Evolution of the TMR ratio as a function of thickness of the bottom $CoFeB_1$ free layer. Error bars represent the standard deviation calculated from measurements of 10 devices.

defined as $\mathrm{TMR}(\%) = (R_{AP} - R_P)/R_P \times 100\%$, where R_P and R_{AP} are resistances of the MTJ when the magnetization configurations of the free and reference layers are completely parallel and antiparallel, respectively. To obtain the major TMR loops, the measurement is conducted over a wide magnetic field range to switch the pinned reference layer (±3.0 kOe). When scanning the magnetic field from the negative direction, the TMR curve first rises to the high-resistance state (R_{AP}) by switching the magnetization of the reference layer. As shown in left panel of Fig. 3(a)–3(d), the switching field of the reference layer slightly decreases with the increased thickness of the bottom $CoFeB_1$ free layer. Upon further increasing magnetic fields, the bottom $CoFeB_1$ free layer switches together with the skyrmion multilayer between ±0.6 kOe, as a result of ferromagnetic interlayer coupling between them.

Through fixing the magnetization orientation of the reference layer after negative saturation, and then sweeping the field between ±0.8 kOe, the corresponding minor loops are subsequently measured. In contrast to the standard perpendicularly magnetized MTJs that exhibit two-level switching between the parallel and antiparallel (R_P and R_{AP}) magnetization states,[31,33,35,36] intermediate TMR steps emerge during the switching process. Note that the spin-dependent tunneling of electrons that leads to TMR is only sensitive to the (planar) magnetization configuration of the CoFeB free layers that located on the opposite sides of MgO tunneling barrier.[47,51,52] Since the magnetization of the $CoFeB_2$ reference layer is fixed in minor loop measurement, these intermediate TMR states suggest the presence of multi-domain state in the $CoFeB_1$ free layer. This can be understood from the ferromagnetic interlayer coupling between the bottom $CoFeB_1$ free layer and the $[Pt/Co/Ta]_{10}$ skyrmion multilayers, which imprint the nanometric skyrmions from $[Pt/Co/Ta]_{10}$ into the bottom $CoFeB_1$ free layer.[49,51,55] Notably, the shape of minor loop of the MTJ device that is made of the 0.9 nm-thick $CoFeB_1$ free layer is consistent with the M-H loop of the bottom $[Pt/Co/Ta]_{10}$ multilayer. This indicates a ferromagnetic interlayer coupling that ensures an imprinting of nanoscale skyrmions into the $CoFeB_1$ free layer. On the contrary, the MTJ device that is made of the 1.05 nm-thick $CoFeB_1$ free layer shows an extra switching event, as evidenced from its minor loop. The MTJ devices with free layer thickness of 1.1 nm and 1.15 nm show neither skyrmion phase nor PMA. These data suggest that a 0.9 nm-thick $CoFeB_1$ free layer is capable of establishing both the PMA and the ferromagnetic interlayer coupling with the underneath $[Pt/Co/Ta]_{10}$ skyrmion multilayer. Based on which, further optimization will be conducted. Summarized in Fig. 3(e) is the evolution of TMR ratio as a function of the thickness of the bottom $CoFeB_1$ free layer. Error bars represent the standard deviation calculated from measurements of over 10 devices. There, one can find that the TMR ratio exceeds 100% in devices made of a 0.9 nm-thick $CoFeB_1$ layer and decreases following the increased thickness of the bottom $CoFeB_1$ layer.

TMR Variation with Annealing Temperatures. Next, we examine the influence of annealing temperature on the TMR ratio of the skyrmionic MTJs made of Ta(5)/[Pt(2.5)/Co(1)/Ta(0.5)]$_9$/Pt(2.5)/Co(1)/Ta(1) /$CoFeB_1$(0.9)/MgO(1.7)/$CoFeB_2$(1.1)/Ta(0.5)/SAF. On the one hand, proper choice of annealing temperature

could promote the crystallization of the MgO layer, which facilitates the spin-dependent tunneling of electrons between the magnetic layers and subsequently enhances the TMR ratio.[31,33,36] On the other hand, increased annealing temperature accelerates diffusion of the constituent elements such as B, leading to a decreased TMR ratio.[33,35,69] It is thus demanded to optimize the annealing temperature for achieving the maximized TMR ratio in the skyrmionic MTJ devices. To fulfill this target, eight identical pieces of devices are annealed under vacuum at 100, 200, 250, 275, 300, 325, and 350 ℃ for one hour, respectively, with one device remaining unannealed as a control sample.

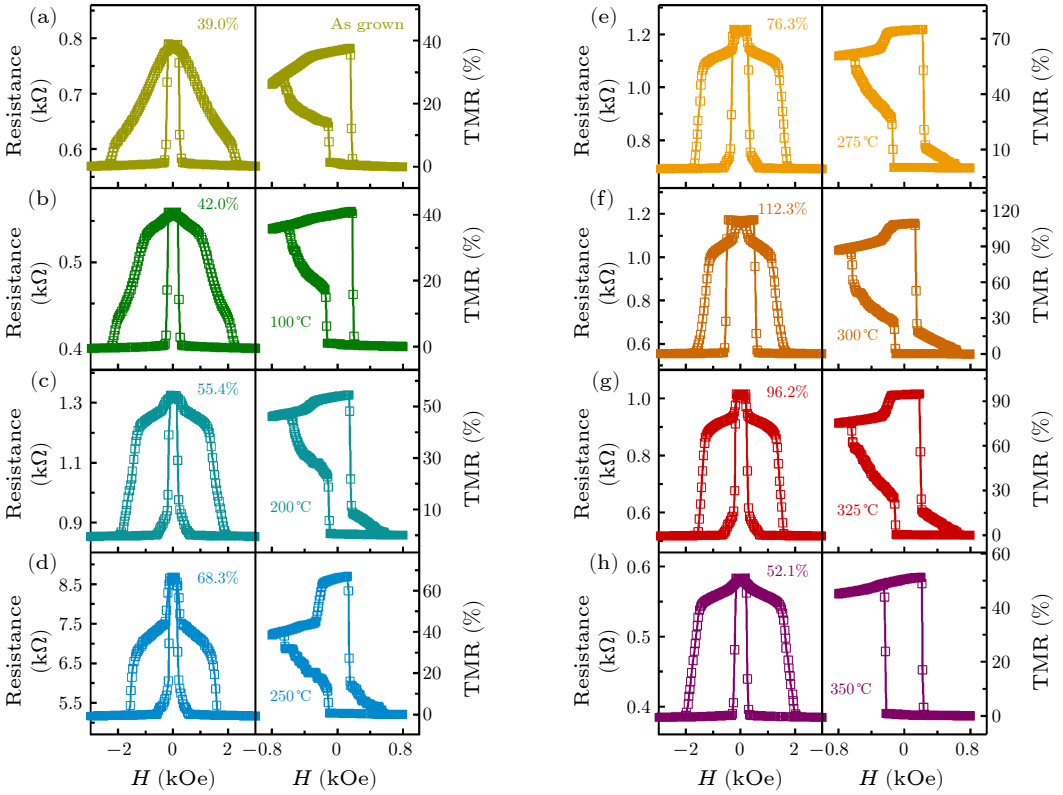

Fig. 4. (a)–(h) Out-of-plane major (left) and minor (right) TMR loops for MTJ devices annealed at different temperatures. These MTJ devices are made of the Ta(5)/[Pt(2.5)/Co(1)/Ta(0.5)]$_9$/Pt(2.5)/Co(1)/Ta(1)/CoFeB$_1$(0.9)/MgO(1.7)/CoFeB$_2$(1.1)/Ta(0.5)/SAF multilayers. The annealing temperature and the corresponding TMR ratio are accordingly labeled.

The major and minor TMR loops are measured and plotted in Figs. 4(a)–4(h), in which the corresponding annealing temperatures and TMR ratios are labeled accordingly. It is reported that the annealing process could significantly enhance the PMA of the reference layer.[69–71] In the as-grown skyrmionic MTJ device (no annealing), the reference layer undergoes a gradual switching with the magnetic field. This suggests that the reference layer exhibits an in-plane magnetic anisotropy, as shown in the major loop on the left. As the annealing temperature increases, PMA in the reference layer is gradually established, leading to changes in the shape of the TMR curves. The reference layer exhibits a sharp switching from 275 ℃ and sustains this characteristic up to 350 ℃, indicating the presence of PMA in the reference layer, as shown in the right panel of Fig. 4. Minor loop measurements allow a detailed analysis of the magnetization dynamics in the CoFeB$_1$ free layer. Notably, minor loops for MTJ devices annealed at temperatures between 200–325 ℃ show consistency with the M-H loop of the bottom [Pt/Co/Ta]$_{10}$ multilayer, indicating an imprinting of spin texture from the [Pt/Co/Ta]$_{10}$ multilayer into the CoFeB$_1$ free layer.

Figure 5 summarizes the evolution of TMR ratio, which shows a nonmonotonic increase as a function of the annealing temperature. Following the increase of the annealing temperature, TMR ratios first monotonically

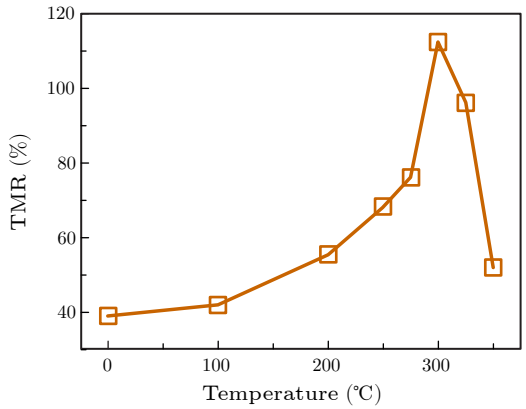

Fig. 5. Evolution of the TMR ratio as a function of annealing temperature, which reaches a maximum of 112.3% for the MTJ devices annealed at 300 ℃.

increase and reach a maximum of 112.3% for MTJ devices annealed at 300 ℃. Above 300 ℃, a decrease of the TMR ratio is observed. Such behaviors can be attributed to the atomic intermixing between the layers, which are consistent with typical $CoFeB_1/MgO/CoFeB_2$-based MTJs.[33,36,69,70,72]

Summary. We have studied the optimization of skyrmion hosting multilayers $[Pt/Co/Ta]_{10}$ with the perpendicularly magnetized $CoFeB_1/MgO/CoFeB_2$ MTJs to achieve an electrical detection of room-temperature skyrmions by TMR. In particular, a series of multilayers of stacking order and composition: $Ta(5)/[Pt(2.5)/Co(1)/Ta(0.5)]_9/Pt(2.5)/Co(1)/Ta(t_{Ta}, \text{spacer})/CoFeB_1(t_{CoFeB_1})/MgO(1.7)/CoFeB_2(t_{CoFeB_2})/Ta(0.5)/Co(0.3)/[Pt(1.5)/Co(0.4)]_2/Ru(0.85)/[Co(0.5)/Pt(1.5)]_3/Ru(5)$ have been systematically deposited and examined. By changing the thickness of the Ta spacer between $[Pt/Co/Ta]_{10}$ and $CoFeB_1/MgO/CoFeB_2$ stacks, we have successfully established a ferromagnetic interlayer coupling that ensures an imprinting of skyrmionic spin textures into the bottom $CoFeB_1$ free layer of the perpendicularly magnetized MTJ. Through studying the thickness of the bottom $CoFeB_1$ layer, we have identified that the MTJ device of a 0.9 nm-thick $CoFeB_1$ free layer shows a strong ferromagnetic interlayer coupling within the hybrid free layer and achieves over 100% TMR ratio at room temperature. We further studied the effect of annealing temperature on the TMR ratio, and found that MTJ devices that were annealed at 300 ℃ exhibit both the enhanced perpendicular magnetic anisotropy and the maximized TMR ratio of 112.3%. Our optimization strategy of the top-pinned skyrmionic MTJ stacks could ensure an efficient TMR detection of nanoscale and mobile skyrmions at room temperature, which can promote the technological application of skyrmionic devices.

Acknowledgements. The work carried out at Tsinghua University is supported by the National Key R&D Program of China (Grant No. 2022YFA1405100), the NSFC distinguished Young Scholar program (Grant No. 12225409), the Basic Science Center Project of National Natural Science Foundation of China (NSFC) (Grant No. 52388201), the NSFC general program (Grant Nos. 52271181, 51831005, and 12421004), the Innovation Program for Quantum Science and Technology (Grant No. 2023ZD0300500), and Beijing Natural Science Foundation (Grant No. Z240006). The work carried out at King Abdullah University of Science and Technology (KAUST) is supported by the KAUST Office of Sponsored Research (OSR) under Award Nos. ORA-CRG10-2021-4665 and ORA-CRG11-2022-5031. Aitian Chen is supported by the National Key Research and Development Program of China (No. 2024YFA1408503) and Sichuan Province Science and Technology Support Program (No. 2025YFHZ0147).

References

[1] Rößler U K, Bogdanov A N, and Pfleiderer C 2006 *Nature* **442** 797
[2] Mühlbauer S, Binz B, Jonietz F, Pfleiderer C, Rosch A, Neubauer A, Georgii R, and Böni P 2009 *Science* **323** 915
[3] Yu X Z, Onose Y, Kanazawa N, Park J H, Han J H, Matsui Y, Nagaosa N, and Tokura Y 2010 *Nature* **465** 901
[4] Nagaosa N and Tokura Y 2013 *Nat. Nanotechnol.* **8** 899
[5] Fert A, Cros V, and Sampaio J 2013 *Nat. Nanotechnol.* **8** 152
[6] Zhang X, Ezawa M, and Zhou Y 2015 *Sci. Rep.* **5** 9400
[7] Wiesendanger R 2016 *Nat. Rev. Mater.* **1** 16044
[8] Jiang W J, Chen G, Liu K, Zang J D, te Velthuis S G E, and Hoffmann A 2017 *Phys. Rep.* **704** 1
[9] Fert A, Reyren N, and Cros V 2017 *Nat. Rev. Mater.* **2** 17031
[10] Everschor-Sitte K, Masell J, Reeve R M, and Kläui M 2018 *J. Appl. Phys.* **124** 240901
[11] Song K M, Jeong J S, Pan B, Zhang X, Xia J, Cha S, Park T E, Kim K, Finizio S, Raabe J, Chang J, Zhou Y, Zhao W, Kang W, Ju H, and Woo S 2020 *Nat Electron* **3** 148
[12] Psaroudaki C and Panagopoulos C 2021 *Phys. Rev. Lett.* **127** 067201
[13] Jin Z, Song M, Fang H, Chen L, Chen J, and Tao Z 2022 *Chin. Phys. Lett.* **39** 108502
[14] Jiang W J, Upadhyaya P, Zhang W, Yu G Q, Jungfleisch M B, Fradin F Y, Pearson J E, Tserkovnyak Y, Wang K L, Heinonen O, te Velthuis S G E, and Hoffmann A 2015 *Science* **349** 283
[15] Woo S, Litzius K, Kruger B, Im M Y, Caretta L, Richter K, Mann M, Krone A, Reeve R M, Weigand M, Agrawal P, Lemesh I, Mawass M A, Fischer P, Klaui M, and Beach G R S D 2016 *Nat. Mater.* **15** 501
[16] Legrand W, Maccariello D, Reyren N, Garcia K, Moutafis C, Moreau-Luchaire C, Collin S, Bouzehouane K, Cros V, and Fert A 2017 *Nano Lett.* **17** 2703
[17] Soumyanarayanan A, Raju M, Gonzalez Oyarce A L, Tan A K C, Im M Y, Petrović A P, Ho P, Khoo K H, Tran M, Gan C K, Ernult F, and Panagopoulos C 2017 *Nat. Mater.* **16** 898
[18] Maccariello D, Legrand W, Reyren N, Garcia K, Bouzehouane K, Collin S, Cros V, and Fert A 2018 *Nat. Nanotechnol.* **13** 233
[19] Liu J H, Wang Z D, Xu T, Zhou H G, Zhao L, Je S G, Im M Y, Fang L, and Jiang W J 2022 *Chin. Phys. Lett.* **39** 017501
[20] Kern L M, Pfau B, Deinhart V, Schneider M, Klose C, Gerlinger K, Wittrock S, Engel D, Will I, Günther C M, Liefferink R, Mentink J H, Wintz S, Weigand M, Huang M J, Battistelli R, Metternich D, Büttner F, Höflich K, and Eisebitt S 2022 *Nano Lett.* **22** 4028
[21] Tang J, Wu Y, Jiang J, Kong L, Liu W, Wang S, Tian M, and Du H 2023 *Sci. Bull.* **68** 2919
[22] Zeissler K, Finizio S, Shahbazi K, Massey J, Al Ma'Mari F, Bracher D M, Kleibert A, Rosamond M C, Linfield E H, Moore T A, Raabe J, Burnell G, and Marrows C H 2018 *Nat. Nanotechnol.* **13** 1161
[23] Hirschberger M, Spitz L, Nomoto T, Kurumaji T, Gao S, Masell J, Nakajima T, Kikkawa A, Yamasaki Y, Sagayama H, Nakao H, Taguchi Y, Arita R, Arima T H, and Tokura Y 2020 *Phys. Rev. Lett.* **125** 076602
[24] Wang Z, Guo M, Zhou H A, Zhao L, Xu T, Tomasello R, Bai H, Dong Y, Je S G, Chao W, Han H S, Lee S, Lee K S, Yao Y, Han W, Song C, Wu H, Carpentieri M, Finocchio G, Im M Y, Lin S Z, and Jiang W 2020 *Nature Electronics* **3** 672
[25] Fernández Scarioni A, Barton C, Corte-León H, Sievers S, Hu X, Ajejas F, Legrand W, Reyren N, Cros V, Kazakova O, and Schumacher H W 2021 *Phys. Rev. Lett.* **126** 077202
[26] Hanneken C, Otte F, Kubetzka A, Dupé B, Romming N, von Bergmann K, Wiesendanger R, and Heinze S 2015 *Nat. Nanotechnol* **10** 1039

[27] Du H, Liang D, Jin C, Kong L, Stolt M J, Ning W, Yang J, Xing Y, Wang J, Che R, Zang J, Jin S, Zhang Y, and Tian M 2015 *Nat. Commun.* **6** 7637

[28] Crum D M, Bouhassoune M, Bouaziz J, Schweflinghaus B, Blügel S, and Lounis S 2015 *Nat. Commun.* **6** 8541

[29] Aqeel A, Azhar M, Vlietstra N, Pozzi A, Sahliger J, Huebl H, Palstra T T M, Back C H, and Mostovoy M 2021 *Phys. Rev. B* **103** L100410

[30] Julliere M 1975 *Phys. Lett. A* **54** 225

[31] Parkin S S, Kaiser C, Panchula A, Rice P M, Hughes B, Samant M, and Yang S H 2004 *Nat. Mater.* **3** 862

[32] Li F F, Jiang L X, Sharif R, Zhang X Q, Feng Y Q, and Han X F 2005 *Chin. Phys. Lett.* **22** 2043

[33] Ikeda S, Miura K, Yamamoto H, Mizunuma K, Gan H D, Endo M, Kanai S, Hayakawa J, Matsukura F, and Ohno H 2010 *Nat. Mater.* **9** 721

[34] Gu X R, Guo L D, and Sun X N 2018 *Chin. Phys. B* **27** 107202

[35] Hayakawa J, Ikeda S, Lee Y M, Matsukura F, and Ohno H 2006 *Appl. Phys. Lett.* **89** 232510

[36] Ikeda S, Hayakawa J, Ashizawa Y, Lee Y M, Miura K, Hasegawa H, Tsunoda M, Matsukura F, and Ohno H 2008 *Appl. Phys. Lett.* **93** 082508

[37] Ikeda S, Sato H, Honjo H, Enobio E C I, Ishikawa S, Yamanouchi M, Fukami S, Kanai S, Matsukura F, Endoh T, and Ohno H 2014 *IEEE International Electron Devices Meeting* p. 33.2.1

[38] Lee S E, Shim T H, and Park J G 2016 *NPG Asia Materials* **8** e324

[39] Dieny B, Prejbeanu I L, Garello K, Gambardella P, Freitas P, Lehndorff R, Raberg W, Ebels U, Demokritov S O, Akerman J, Deac A, Pirro P, Adelmann C, Anane A, Chumak A V, Hirohata A, Mangin S, Valenzuela S O, Onbaşlı M C, d'Aquino M, Prenat G, Finocchio G, Lopez-Diaz L, Chantrell R, Chubykalo-Fesenko O, and Bortolotti P 2020 *Nature Electronics* **3** 446

[40] Koshibae W, Kaneko Y, Iwasaki J, Kawasaki M, Tokura Y, and Nagaosa N 2015 *Jpn. J. Appl. Phys.* **54** 053001

[41] Zhang X, Cai W, Zhang X, Wang Z, Li Z, Zhang Y, Cao K, Lei N, Kang W, Zhang Y, Yu H, Zhou Y, and Zhao W 2018 *ACS Applied Materials & Interfaces* **10** 16887

[42] Kasai S, Sugimoto S, Nakatani Y, Ishikawa R, and Takahashi Y K 2019 *Appl. Phys. Expr.* **12** 083001

[43] Penthorn N E, Hao X, Wang Z, Huai Y, and Jiang H W 2019 *Phys. Rev. Lett.* **122** 257201

[44] Schäfer-Richarz J F, Risius P, Czerner M, and Heiliger C 2019 *Phys. Rev. B* **100** 214413

[45] Alamdar M, Leonard T, Cui C, Rimal B P, Xue L, Akinola O G, Patrick Xiao T, Friedman J S, Bennett C H, Marinella M J, and Incorvia J A C 2021 *Appl. Phys. Lett.* **118** 112401

[46] Raymenants E, Bultynck O, Wan D, Devolder T, Garello K, Souriau L, Thiam A, Tsvetanova D, Canvel Y, Nikonov D E, Young I A, Heyns M, Soree B, Asselberghs I, Radu I, Couet S, and Nguyen V D 2021 *Nat. Electron* **4** 392

[47] Chen H, Bouckaert W, and Majetich S A 2022 *J. Magn. Magn. Mater.* **541** 168552

[48] Li S, Du A, Wang Y, Wang X, Zhang X, Cheng H, Cai W, Lu S, Cao K, Pan B, Lei N, Kang W, Liu J, Fert A, Hou Z, and Zhao W 2022 *Sci. Bull.* **67** 691

[49] Guang Y, Zhang L, Zhang J, Wang Y, Zhao Y, Tomasello R, Zhang S, He B, Li J, Liu Y, Feng J, Wei H, Carpentieri M, Hou Z, Liu J, Peng Y, Zeng Z, Finocchio G, Zhang X, Coey J M D, Han X, and Yu G 2023 *Adv. Electron. Mater.* **9** 2200570

[50] He B, Hu Y, Zhao C, Wei J, Zhang J, Zhang Y, Cheng C, Li J, Nie Z, Luo Y, Zhou Y, Zhang S, Zeng Z, Peng Y, Coey J M D, Han X, and Yu G 2023 *Adv. Electron Mater* **9** 2201240

[51] Chen S, Lourembam J, Ho P, Toh A K J, Huang J, Chen X, Tan H K, Yap S L K, Lim R J J, Tan H R, Suraj T S, Sim M I, Toh Y T, Lim I, Lim N C B, Zhou J, Chung H J, Lim S T, and Soumyanarayanan A 2024 *Nature* **627** 522

[52] Urrestarazu Larrañaga J, Sisodia N, Guedas R, Pham V T, Di Manici I, Masseboeuf A, Garello K, Disdier F, Fernandez B, Wintz S, Weigand M, Belmeguenai M, Pizzini S, Sousa R C, Buda-Prejbeanu L D, Gaudin G, and Boulle O 2024 *Nano Lett.* **24** 3557

[53] Zhao M, Chen A, Huang P Y, Liu C, Shen L, Liu J, Zhao L, Fang B, Yue W C, Zheng D, Wang L, Bai H, Shen K, Zhou Y, Wang S, Liu E, He S, Wang Y L, Zhang X, and Jiang W 2024 *npj Quantum Mater.* **9** 50

[54] Yang H X, Chshiev M, Dieny B, Lee J H, Manchon A, and Shin K H 2011 *Phys. Rev. B* **84** 054401

[55] Nandy A K, Kiselev N S, and Blügel S 2016 *Phys. Rev. Lett.* **116** 177202

[56] Liu E, Wu Y C, Couet S, Mertens S, Rao S, Kim W, Garello K, Crotti D, Van Elshocht S, De Boeck J, Kar G S, and Swerts J 2018 *Phys. Rev. Appl.* **10** 054054

[57] Wang W G, Li M, Hageman S, and Chien C L 2012 *Nature Materials* **11** 64

[58] Zhang S, Zhang J, Wen Y, Chudnovsky E M, and Zhang X 2018 *Appl. Phys. Lett.* **113** 192403

[59] Moreau-Luchaire C, Mouta S C, Reyren N, Sampaio J, Vaz C A, Van Horne N, Bouzehouane K, Garcia K, Deranlot C, Warnicke P, Wohlhuter P, George J M, Weigand M, Raabe J, Cros V, and Fert A 2016 *Nat. Nanotechnol.* **11** 444

[60] Liu E, Swerts J, Couet S, Mertens S, Tomczak Y, Lin T, Spampinato V, Franquet A, Van Elshocht S, Kar G, Furnemont A, and De Boeck J 2016 *Appl. Phys. Lett.* **108** 132405

[61] Liu E, Swerts J, Vaysset A, Devolder T, Couet S, Mertens S, Lin T, Elshocht S V, Boeck J D, and Kar G S 2017 *IEEE International Magnetics Conference* p. 1

[62] Moriyama T, Ni C, Wang W G, Zhang X, and Xiao J Q 2006 *Appl. Phys. Lett.* **88** 222503

[63] Zhang S, Zhang J, Wen Y, Chudnovsky E M, and Zhang X 2018 *Commun. Phys.* **1** 36

[64] Wang L, Liu C, Mehmood N, Han G, Wang Y, Xu X, Feng C, Hou Z, Peng Y, Gao X, and Yu G 2019 *ACS Applied Materials & Interfaces* **11** 12098

[65] Pollard S D, Garlow J A, Yu J, Wang Z, Zhu Y, and Yang H 2017 *Nat. Commun.* **8** 14761

[66] Singh J P, Bhardwaj R, Sharma A, Kaur B, Won S O, Gautam S, and Chae K H 2019 *Adv. Appl. Manuf. Eng.* p. 53

[67] Lee D Y, Hong S H, Lee S E, and Park J G 2016 *Sci. Rep.* **6** 38125

[68] Nistor L E, Rodmacq B, Auffret S, and Dieny B 2009 *Appl. Phys. Lett.* **94** 012512

[69] Schnitzspan L, Cramer J, Kubik J, Tarequzzaman M, Jakob G, and Kläui M 2020 *IEEE Magn. Lett.* **11** 1

[70] Meng H, Sbiaa R, Wang C C, Lua S Y H, and Akhtar M A K 2011 *J. Appl. Phys.* **110** 103915

[71] Caseiro M, Macedo R, Araujo P D R, Cardoso S, Erkovan M, and Freitas P P 2023 *J. Mater. Sci.: Mater. Electron.* **34** 1671

[72] Kim G, Lee S, Lee S, Song B, Lee B K, Lee D, Lee J S, Lee M H, Kim Y K, and Park B G 2023 *Nanomaterials* **13** 2591